Does the use of load-reducing IPC on a wake-steering turbine affect wake behavior?

C Wang, F Campagnolo, and C L Bottasso

Wind Energy Institute, Technische Universität München, Boltzmannstraße 15, D-85748 Garching bei München, Germany

E-mail: carlo.bottasso@tum.de

Abstract.

This paper aims at quantifying and explaining the effects of Individual Pitch Control (IPC) on the wake of a wake-steering wind turbine. As the machine is intentionally misaligned with respect to the wind, IPC can be used to mitigate the resulting extra loading. However, while IPC reduces loads, it also affects the wake, which influences the power of downstream turbines. The question is therefore whether the IPC activity has any other appreciable effect at the wind farm level, in addition to its original turbine-level load reduction goal. In this work, experiments and CFD simulations of scaled wind turbines in a boundary layer wind tunnel are considered. The CFD model is first validated with measurements, and then used to show subtle changes in the wake, power and loads caused by IPC. It is observed that IPC does indeed have some non-negligible effects, and that these effects differ for positive and negative yawing.

1. Introduction

Although IPC increases pitch activity and affects the duty cycle, it reduces the periodic loads caused by shear and wind misalignment, resulting in reduced fatigue damage [1]. Furthermore, blade-passing 3P loads [2, 3] and aerodynamic or mass imbalances of the rotor can also be mitigated by IPC [4]. Today, operation at high misalignment angles is actively investigated as a way to control the wake path, with potential benefits in terms of power capture and loading of downstream wind turbines [5, 6]. However, the high misalignment angles at which a wake-steering machine must operate may induce an increase in fatigue loading, and IPC can be used to limit this negative effect of wake steering. The present paper tries to answer the following questions: if IPC is used to reduce the loads on a wake-steering turbine, what is the effect on the wake? Are path and/or recovery affected? Are these effects beneficial or detrimental for the downstream machine? And are the loads on the wake-steering turbine significantly reduced?

2. Methodology

2.1. Experimental setup

The questions posed above are investigated in this paper by using both ad hoc wind tunnel experiments and a simulation model. Two scaled wind turbines of the G1 type [7,8] were installed in the large boundary layer wind tunnel of the Politecnico di Milano, one 5D downstream of the other. Both turbines were equipped with a standard collective pitch-torque controller, with an optional IPC loop. A sheared inflow with a 5% turbulence intensity was generated in the

wind tunnel by passive means using a cluster of spires, resulting in a shear power coefficient of about 0.12. One test was conducted by removing the downstream turbine, with the goal of characterizing at its location the wake of the upstream machine using hot wire probes.

2.2. Simulation model

The simulation model is developed with a Large Eddy Simulator (LES) coupled with an Actuator Line Method (ALM), described in [5, 9]. While ALM is used to model blades, the Immersed Boundary Method (IBM) is used to model the nacelle and tower. To reduce the computational cost, a Scale Adaptive Simulation (SAS) was also often used, with practically the same results as LES. The turbulent inflow was obtained by LES precursor simulations conducted with Foam-extend [11] using a structured body-conforming mesh of the spires and the wind tunnel, as described in greater detail in [6].

2.3. Turbine control

The IPC implementation is based on fixed-frame loads, obtained by transforming rotating-frame measurements provided by strain gages installed on the shaft of the G1 machines. The pitch inputs in the d-q coordinate system are computed by a proportional-integral controller. The reference angles in the d-q coordinate system β_d, β_q are governed by a PI controller:

$$\beta_d = K_I \int_0^t M_n(\tau) d\tau + K_P M_n(t), \tag{1a}$$

$$\beta_q = K_I \int_0^t M_y(\tau) d\tau + K_P M_y(t), \tag{1b}$$

where K_I , K_P are integral and propotional gains, respectively, and M_n and M_y are the fixed frame nodding and yawing moments. The inverse Coleman transformation is then used to obtain the blade pitch angles from the d-q frame [1]:

$$\beta_i(\psi_i) = \beta_d \cos(\psi_i) + \beta_q \sin(\psi_i), \tag{2}$$

where ψ_i is the azimuth angle of each blade, $\psi = 0^\circ$ corresponding to the blade pointing vertically up, and ψ increases clockwise when looking downstream. The total pitch angle of each blade is the sum of its individual pitch angle β_i and the collective pitch angle β_c.

The baseline generator torque controller is based on a standard look-up table, while the collective pitch angle is constant since turbines only operate in region 2. The same controllers have been implemented in simulations and experiments.

3. Results

3.1. Validation of CFD

To digitally duplicate the experiments, it is necessary to accurately simulate the inflow in the wind tunnel. In fact, turbulence intensity influences wake recovery, while wind shear affects the IPC behavior. In the tunnel, turbulence was generated passively with an array of spires. The generated turbulent flow field has both a vertical and a small lateral wind shear. The turbulence intensity of 5% and the vertical wind shear equal to 0.12 obtained by the precursor simulation are both very close to the measurements.

Figure 1 illustrates the flow at hub height for two simulations considering only the upstream turbine, at 30° yaw (left plot) and 0° yaw (right plot). The dashed lines indicate the position of the downstream wind turbine that is 5D away from the upstream one.

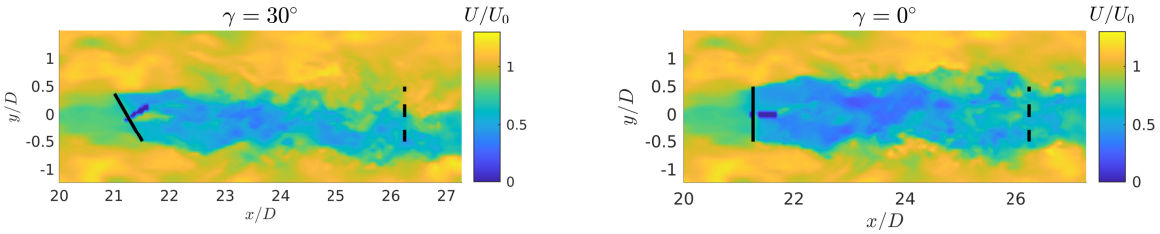

Figure 1: Top view of the instantaneous longitudinal flow speed at hub height. Solid lines indicate the upstream rotor, while dashed lines the downstream one.

Figure 2 shows the pitch angle of the first blade as a function of its azimuth for the $\gamma = 0°$ case. The pitch angle is not a single-valued function of the azimuth because of turbulence and rotor dynamics. However, the data points form a sinusoidal shape with its lowest value around $\psi_1 = 180°$. The scatter of the experimental data points is slightly bigger than the one of the simulations, which is probably mainly caused by measurement noise in the experiments or by having neglected the elasticity of the blades in the simulations.

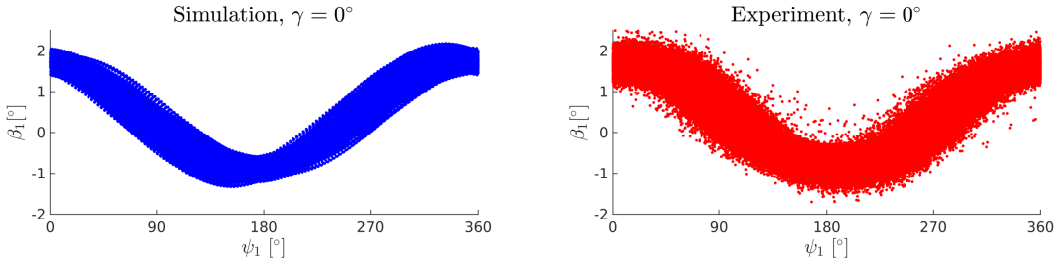

Figure 2: Comparison of the pitch angle of the first blade between simulation and experiment for the zero-yaw case.

To obtain a clearer view of the pitch-azimuth relationship, the mean pitch value corresponding to each azimuthal angle was calculated for each operating condition, as shown in Fig. 3. Table 1 shows the mean values of β_d, β_q and also the changes in loads and power caused by IPC.

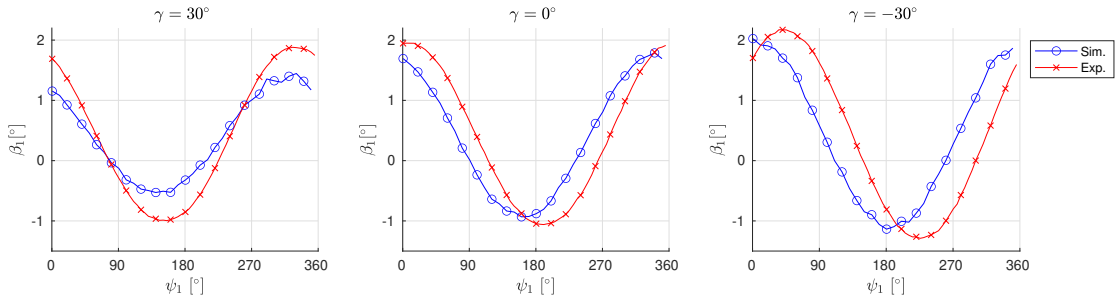

Figure 3: Comparison of average individual pitch behavior for different yaw misalignment cases.

	$\gamma = 30°$		$\gamma = 0°$		$\gamma = -30°$	
Data source	CFD	EXP	CFD	EXP	CFD	EXP
$\Delta\lvert\bar{M}_n\rvert/\lvert\bar{M}_n\rvert$	-99%	-94%	-99%	-99%	-99%	-99%
$\Delta\lvert\bar{M}_y\rvert/\lvert\bar{M}_y\rvert$	-97%	-95%	-81%	-88%	-98%	-98%
β_d [°]	0.90	1.27	1.28	1.36	1.45	1.21
β_q [°]	-0.67	-0.55	0.09	0.34	0.40	1.19
$\Delta C_P/C_P$	+1.0%	+1.5%	-3.0%	-0.4%	-2.6%	-1.8%

Table 1: Pitch angles and changes in power and fixed frame (nodding and yawing) moments for different yaw misalignment cases.

Note that IPC is not typically used in region 2 in aligned ($\gamma = 0°$) conditions, because of its impact on actuator duty cycle. However, here it is assumed that IPC is used in region 2 to mitigate the extra fatigue caused by yaw misalignment for wake-steering wind farm control.

There are some differences between simulations and experiments in the mean values of β_d and β_q, which are mainly driven by the differences in the vertical and horizontal local wind shears, respectively. In fact, although the inflow speed distribution in the simulation is very similar to the one of the experiments, the two are still not exactly identical. Notwithstanding these small differences, the experimental measurements can still be used as references for the simulations, since the goal of this work is to investigate changes caused by IPC rather than a precise match between experiments and simulations. Indeed, experiments and simulations show many similar trends.

In fact, changes in the yaw angle γ influence the phase of the $\beta - \psi$ curve. For positive yaw angles, the curve shifts to the right, and vice versa. This phenomenon is mainly driven by the change of β_q and it has an aerodynamic explanation. For a zero-yaw turbine with IPC, the pitch angle is smallest when the blade is close to the lower part of the rotor ($\psi = 180°$). When the turbine is yawed by $\gamma = 30°$, the left side ($\psi = 270°$) of the rotor moves upstream, while the right side ($\psi = 90°$) moves downstream. This tends to decrease the angle of attack and loads of the right side of the rotor, because the blade moves into the induction zone of the rotor, where the flow speed is lower. The opposite happens for the left side of the rotor. At this point, IPC intervenes to increase pitch on the left side and decrease pitch on the right side, which results in a negative value of β_q and a left shift of the $\beta - \psi$ curve. The analysis is similar for the other yaw direction ($\gamma = -30°$) and it results in a positive value of β_q and a right shift of the curve. For the zero yaw case, a non-zero β_q is only caused by the local horizontal wind shear, which is slightly larger in the experiment than in the simulations.

Changes in the yaw angle also influence the amplitude of the $\beta - \psi$ curve: the amplitude decreases as γ increases, and vice versa. Although the sensitivity is stronger in simulations, this phenomenon is visible from both simulation and experimental results, as shown in Fig. 3. In the simulation, the difference of β_q in absolute value terms is significant between the $\gamma = 30°$ and $\gamma = 0°$ cases, while the difference is small for the experiment, which is consistent with the significant change of amplitude between these two yaw misalignment cases for the simulation and a smaller change for the experiment. These differences might be caused by a slightly different horizontal shear.

The change in β_q is already understood, the task here is to explain the change in β_d, which can be done with the help of the schematic sketches of Fig. 4. In the figure, the airfoil profile at different azimuthal locations has been shown. The speed of the airfoil caused by the rotor rotation is ΩR. When the turbine is yawed, the incoming flow includes both a normal component $U\cos(\gamma)$ and a tangential component $U\sin(\gamma)$, so that the direction of the flow depends on the yaw direction and magnitude. For the cases with $\gamma = 30°$, $\psi = 0°$ (blade highest position) and

$\gamma = -30°$, $\psi = 180°$ (blade lowest position), the effect of yaw misalignment is to decrease the relative speed V_{Rel} with respect to the airfoil and increase the angle of attack α. In contrast, for the cases with $\gamma = 30°$, $\psi = 180°$ and $\gamma = -30°$, $\psi = 0°$, V_{Rel} increases and α decreases due to yaw. For both yaw misalignment cases, the changes in relative speed and angle of attack have opposite effects on loads. For the operational conditions considered here, the dominant factor is the effect of the relative speed, whose relative change is about 15% between $\psi = 0°$ and $\psi = 180°$, resulting in a 32% relative change of lift. The difference of α between the two azimuthal positions caused by yaw is about 1.0°, which results in only a 13% relative change of lift.

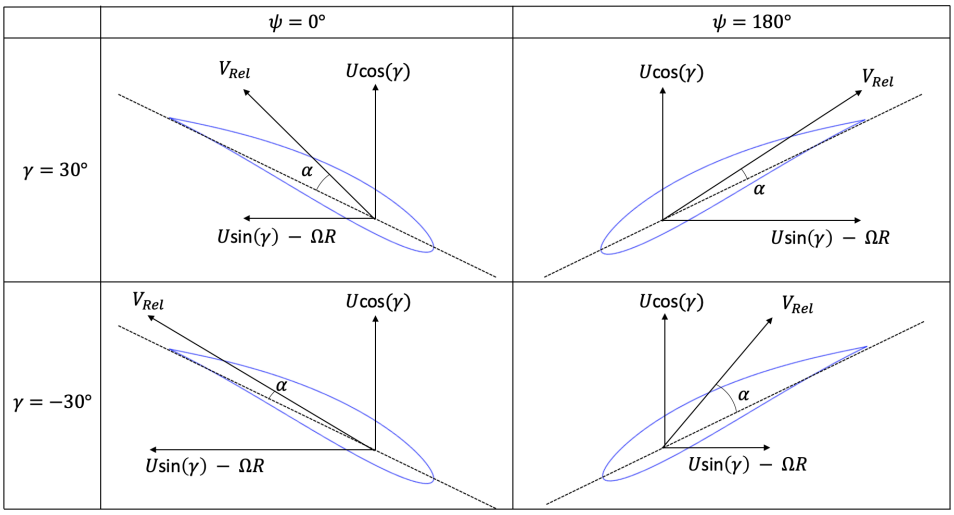

Figure 4: Velocity triangles at different azimuthal positions for different yaw angles. U is the flow speed at the rotor disk; V_{Rel} is the relative speed of the flow with respect to the airfoil; α is the angle of attack.

The presence of a vertical wind shear breaks the symmetry between positive and negative yaw angles. Further analysis of the triangle of velocities shows that a positive vertical shear increases the relative flow speed and angle of attack around $\psi = 0°$, and decreases both quantities around $\psi = 180°$. Considering a negative yaw angle, the effects of yaw and shear both increase the relative speed for $\psi = 0°$, and both decrease it for $\psi = 180°$; on the other hand, the effects on the angle of attack are of an opposite sign and tend to cancel each other. Exactly the opposite happens for a positive yaw angle, where the relative speed changes caused by yaw and shear have opposite signs, while the changes of angle of attack are in the same direction.

These changes in the operating conditions of the airfoils induce an effect of IPC also on power. Indeed, IPC affects power even for $\gamma = 0°$, as shown in Table 1. This is due to the fact that IPC, by aggressively targeting loads, generates an excessively low loading in the top part of the rotor, and an excessively high one in the bottom part. This moves the induction away from the optimal value of 1/3, leading to a loss of power. A similar effect is present when the machine is yawed. However, due to the lack of symmetry and the lower loading for positive yaw angles, IPC leads to a slight power improvement for $\gamma = 30°$ (Table 1).

This lack of symmetry has several effects. In fact, since lift in the top and bottom parts of the rotor changes more for negative than for positive yaw, a higher β_d is required for $\gamma = -30°$ than for $\gamma = 30°$ (cf. Table 1).

In the experiment, horizontal (at hub-height) and vertical wake profiles 5D downstream of the rotor were measured with hot-wire probes. Figure 5 reports the results for the 30° (top

plots), 0° (middle plots) and −30° (bottom plots) yaw misalignment cases. The first and third columns show speed profiles for the case IPC on and off, and for both CFD and experiments. The vertical wake profiles are located at the wake center, which was determined experimentally to be at $Y = -0.405$ m, $Y = 0$ m, and $Y = 0.437$ m for the yaw angles 30°, 0° and -30°, respectively. The match between experiments and simulations is acceptable, and small differences are caused by slight changes in inflow. The second and fourth columns of Fig. 5 show the differences between IPC on and off. Looking at the vertical profiles, it appears that IPC accelerates the flow above hub height and decelerates it below hub height. This effect is proportional to the direct pitch amplitudes β_d, coherently with Table 1. In contrast, the effect of IPC on the horizontal wake profile is not significant, as shown by the fourth column of Fig. 5.

The validation of CFD has been shown from different perspectives, indicating that the numerical model is able to capture the effects of IPC with reasonable accuracy. As the inflow conditions in CFD can be exactly the same for different operating conditions of the turbines, numerical simulations can be used to evaluate subtle differences in power, loading and wake behavior.

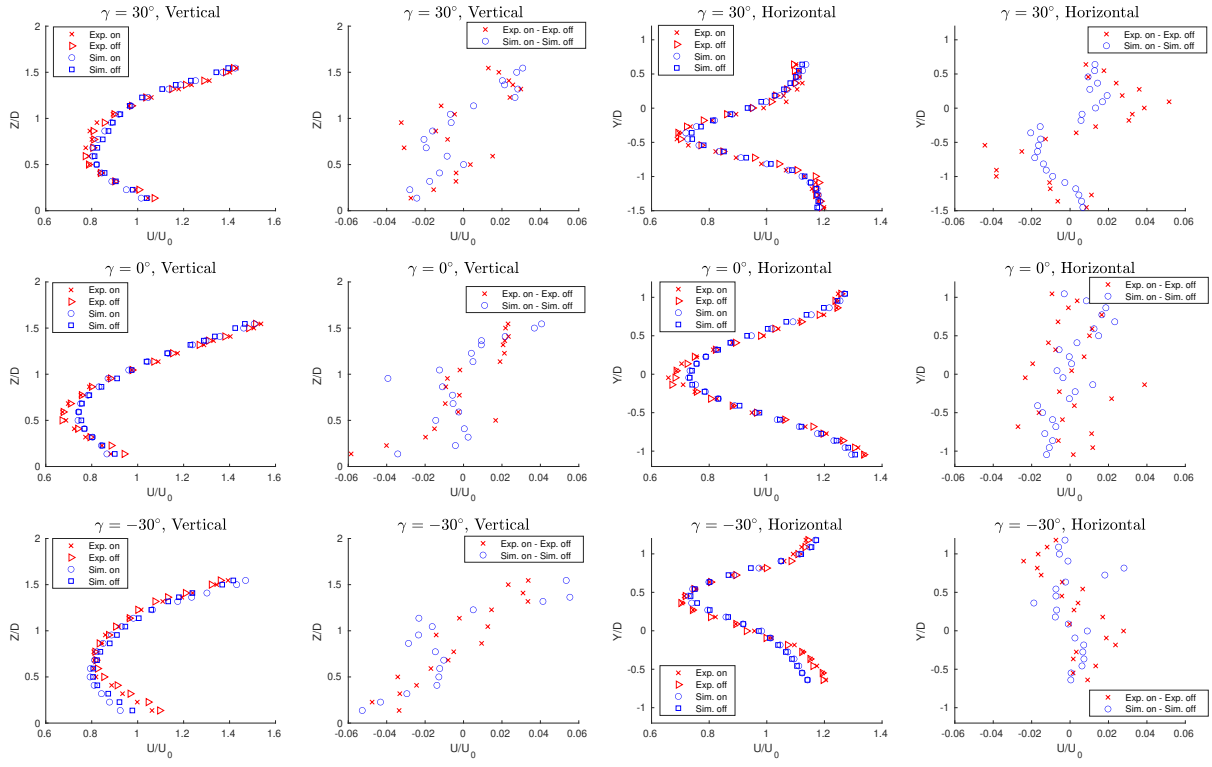

Figure 5: Vertical and horizontal wake profiles with and without IPC, at a 5D downstream location.

3.2. Effects of IPC on wake behavior

Figure 6 shows the difference in the wake longitudinal speed between IPC on and off at a 5D downstream distance, as computed by the simulation model. Looking at the case $\gamma = 0°$, IPC generates an acceleration close to the top of the rotor and a deceleration close to its bottom. This is consistent with the previously noted effect on induction, due to the aggressive targeting of blade loads, which causes a drop in power. As the wake propagates downstream and

swirls clockwise when looking upstream, the acceleration and deceleration regions are convected clockwise around the wake center, as visualized by the high-speed (yellow) and a low-speed (blue) bubbles present in all plots in Fig. 6. For a yawed turbine, a kidney-shaped wake is formed [10], caused by two counter-rotating vortices and the wake swirl. This system of vortices causes a small lateral velocity component on the leeward side of the wake, as shown by Fig. 7. This lateral wind component, indicated with a black arrow in Fig. 6, breaks the high-speed bubble for the $\gamma = 30°$ case and the low-speed bubble for the $\gamma = -30°$ case.

This influences the velocity field, and the resulting changes in the rotor effective wind speeds at the downstream turbine are 0.3%, -1.0% and -0.3% for the 30°, 0° and −30° yaw cases, respectively. By these results, the use of IPC on the upstream turbine is expected to have a positive effect on the power of the downstream turbine for $\gamma = 30°$, while it should have a negative effect for $\gamma = 0°$ and $\gamma = -30°$. These effects are indeed observed in the next subsection, where two turbines are simulated. Notice also that IPC does not seem to have any noticeable effect on wake recovery, as its frequency is not in the neighborhood of typical near-wake unstable modes.

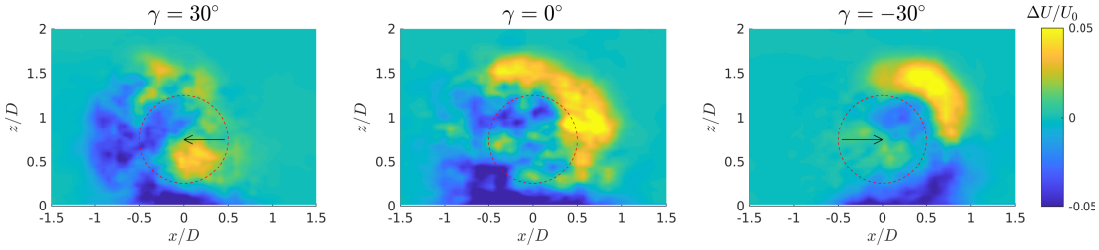

Figure 6: Difference in wake mean longitudinal speed between IPC on and off, 5D downstream of the rotor. The rotor planes are viewed from downstream. The red dashed circles show the location of the downstream rotor.

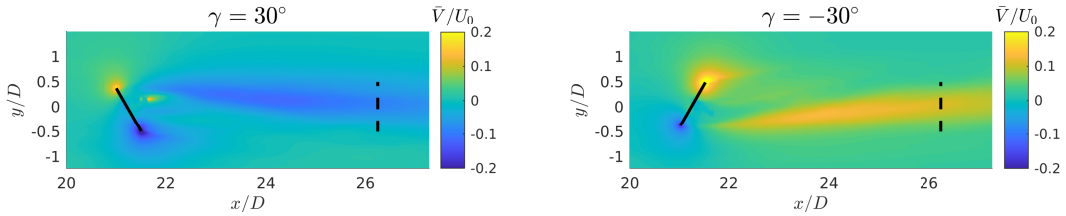

Figure 7: Mean lateral velocity component $\bar{V}$. The lateral velocity is significant only on the leeward side of the wake.

3.3. Effects of upstream turbine IPC

As shown, the activation of IPC on the upstream turbine has effects on both the upstream and downstream machines. Table 2 shows simulation results obtained with two turbines, and reports percentage changes of power coefficient and bending moments. The influence of IPC on the power coefficient C_{P1} of the upstream turbine is consistent with the results of single-turbine simulations shown in Table 1. When $\gamma = 30°$, IPC has a positive effect on the power for both turbines, showing potential for some moderate wind farm power boost. When $\gamma = 0°$, IPC

decreases power of both turbines. This is however not an issue, as IPC is not expected to be used in non-misaligned conditions, due to its negative effect on the actuator duty cycle. When $\gamma = -30°$, power decreases for the first turbine and remains almost constant for the second one.

The mean nodding and yawing moment of the upstream turbine, $|\bar{M}_{y1}|$ and $|\bar{M}_{z1}|$, are reduced to almost zero. The bending moments of the downstream turbine $|\bar{M}_{y2}|$ and $|\bar{M}_{z2}|$ are also slightly influenced, but only to a limited extent.

Case	1	2	3
γ_1 [°]	30	0	-30
WT1 IPC	on	on	on
WT2 IPC	off	off	off
$\Delta C_{P1}/C_{P1}$	+1.7%	-3.0%	-3.9%
$\Delta C_{P2}/C_{P2}$	+1.6%	-4.2%	-0.1%
$\Delta\lvert\bar{M}_{n1}\rvert/\lvert\bar{M}_{n1}\rvert$	-99%	-100%	-100%
$\Delta\lvert\bar{M}_{y1}\rvert/\lvert\bar{M}_{y1}\rvert$	-99%	-94%	-97%
$\Delta\lvert\bar{M}_{n2}\rvert/\lvert\bar{M}_{n2}\rvert$	-6%	-9%	-8%
$\Delta\lvert\bar{M}_{y2}\rvert/\lvert\bar{M}_{y2}\rvert$	+11%	-14%	-2%

Table 2: Effects of the upstream turbine IPC on power and loads. The relative changes of power and mean bending moments with respect to the benchmark cases without IPC are shown. Subscripts 1 and 2 indicate the upstream and downstream turbines, respectively.

3.4. Effects of downstream turbine IPC

Next, the IPC on the downstream turbine is also switched on. The simulated wake profiles at the location of the downstream rotor for both yaw misalignment cases are shown in Fig. 8. Two kidney-shape wakes pointing in opposite directions can be seen in the figure, triggering the response of the IPC controller on the downstream turbine. Table 3 shows the effects of IPC, which, as expected, brings all mean bending moments almost to zero.

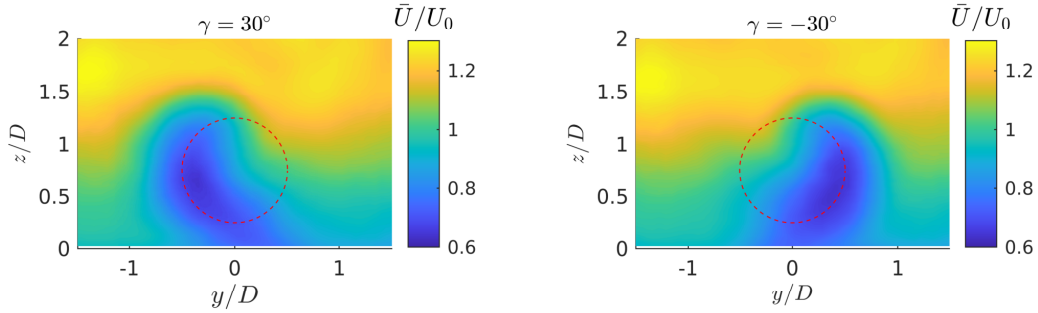

Figure 8: Longitudinal flow speed at the location of the downstream turbine, showing the typical kidney shape of a deflected wake.

When the upstream turbine is not yawed, the downstream turbine is exposed to a full wake. In this case, its power decreases only moderately when IPC is activated, which is the penalty for a high β_d. When the upstream turbine is yawed, there is a partial wake impingement on the downstream turbine, which results in high lateral wind shear. IPC reacts with a high β_q that has a detrimental effect on power; this differs from the beneficial effect of a small β_q discussed in

subsection 3.1. Case 6 indicates a more severe power loss on the downstream turbine than case 4 because of its higher β_d, which is caused by the direction of yaw and can still be explained by the analysis reported in subsection 3.1.

Case	4	5	6
γ_1 [°]	30	0	-30
γ_2 [°]	0	0	0
WT1 IPC	on	on	on
WT2 IPC	on	on	on
β_d [°]	1.5	1.3	1.9
β_d [°]	-2.3	0.2	2.4
$\Delta C_{P2}/C_{P2}$	-8.9%	-3.2%	-13.1%
$\Delta\lvert\bar{M}_{n2}\rvert/\lvert\bar{M}_{n2}\rvert$	-92%	-100%	-96%
$\Delta\lvert\bar{M}_{y2}\rvert/\lvert\bar{M}_{y2}\rvert$	-90%	-90%	-98%

Table 3: Effects on power and loads caused by the use of IPC on the downstream turbine. The relative changes of power and mean bending moments are computed with respect to the corresponding cases 1, 2, 3 of Table 2.

4. Conclusions

The effects caused by the use of IPC on a wake-steering turbine are quantified experimentally and numerically. A simulation model is first validated with experiments and then exploited to study differences caused by IPC on wake behavior, power and loads. The results show that indeed IPC is an effective way of reducing loading for all considered operating conditions. The mechanisms by which IPC influences the turbine and its wake has been discussed. Overall, no significant enhancement of wake recovery has been observed. The use of IPC on the upstream turbine has been shown to generate a moderate power increase for positive yawing, both upstream and downstream, while it induces power losses for negative yawing. IPC on the downstream turbine tends, in general, to always reduce power.

5. Acknowledgements

This work has been supported by the CL-WINDCON project, which receives funding from the European Union Horizon 2020 research and innovation program under grant agreement No. 727477, and by the CompactWind II project (FKZ: 0325492G), which receives funding from the German Federal Ministry for Economic Affairs and Energy (BMWi). The authors also express their appreciation to the Leibniz Supercomputing Centre (LRZ) for providing access and computing time on the SuperMUC-NG System.

References

[1] Bossanyi E A 2003 Individual blade pitch control for load reduction *J. Wind Energy* **6**(2) 119-128
[2] Bossanyi E A 2005 Further load reductions with individual pitch control *J. Wind Energy* **8**(4) 481-485
[3] Selvam K et al. 2009 Feedbackfeedforward individual pitch control for wind turbine load reduction *Int. J. Robust Nonlin.* **19**(1) 72-91
[4] Kanev Stoyan and Van Engelen T G 2009 Exploring the limits in individual pitch control *Pro. of Euro. Wind Energy Conf.* 1-10
[5] Fleming P et al. 2014 Evaluating techniques for redirecting turbine wakes using SOWFA *Renewable Energy* **70** 211-218
[6] Wang C et al. 2018 Validation of large-eddy simulation of scaled waked wind turbines in different yaw misalignment conditions *J. Phys.: Conf. Ser.* **1037**(6) 062007

[7] Campagnolo F et al. 2016 Wind tunnel testing of a closed-loop wake deflection controller for wind farm power maximization *J. Phys.: Conf. Ser.* **753**(3) 032006
[8] Bottasso C L et al. 2014 Wind tunnel testing of scaled wind turbine models: beyond aerodynamics J. Wind Eng. and Ind. Aerodyn. **127** 1128
[9] Wang J et al. 2019 Wake behavior and control: comparison of LES simulations and wind tunnel measurements *Wind Energy Sci.* **4**(1) 71-88.
[10] Bastankhah M and Port-Agel F 2016 Experimental and theoretical study of wind turbine wakes in yawed conditions *J. Fluid Mech.* **806** 506-541
[11] Jasak H 2009 OpenFOAM: open source CFD in research and industry *Int. J. Nav. Arch. Ocean* **1**(2) 89-94